CEIG - Spanish Computer Graphics Conference (2023)
M. Comino and J. Gimeno (Editors)

An adaptative Shader for Human Visual Defects Simulation

Pere Fons[1] Jose Maria Buades[1] and Franisco Perales[1]

[1]Universitat de les Illes Balears
Departamento de Ciencias Matemáticas e Informática

Abstract

A novel programmable shader is proposed to accurately simulate the main important human visual defects under different situations in daily life. An improved model of eye model is introduced to reasonably predict the anatomical and optical properties of the human eye. This eye model is composed of an accommodation and color model, and both these models are combined to simulate the varying refractive power of the human eye and color vision deficiency. Finally, distributed ray tracing techniques is combined with this eye model to produce a variety of visual results using the programmable shader in NVIDIA OptiX environment.

CCS Concepts

• ***Computing methodologies*** → ***Ray tracing;*** • ***Human-centered computing*** → ***Accessibility technologies;***

1. Introduction

Today we have the possibility to simulate accurate human vision properties including the more common defects. We have advanced rendering techniques in computer graphics to simulate in real time the final real image visualized by every individual user. However, the most usual camera lens models in computer graphics are abstract and general, and just suitable for general image synthesis. Simulating real human vision enables very beneficial applications in medicine or eyeglass manufactures, refractive surgery, contact lens design, spectacles design, and so on. To be precise, the lens models must be incorporate the anatomical and optical properties of the human eye to generate consistent visual results with that the human eye really observes. Based on previous research work, we propose a new method to more accurately simulate the visual perception of the human eye under different conditions. We adopt an accurate schematic eye model with the possibility to simulate the accommodation function and adaptative refractive capability of the human eye. Finally using the shaders versatility we combine the images computed in real-time in order to produce synthesized images for simulating the visual perception. The principal defects considered are refractive (myopia, hyperopia, presbyopia or astigmatism), also color perception defects are studied. In order to run our algorithm in real-time we employ massively parallel graphics hardware. The CUDA on NVIDIA cards is used to test our model.

2. Related Work

2.1. Schematic Eye Models

Schematic eye models are very practical in regards to simulation. They are mathematical models that capture how light behaves in the eye environment and its different refractive surfaces. An approach to adapt these models for simulation has been made [WZHX11]. As useful as they are, using detailed models such as Navarro's [NSB85] can heavily affect performance. In [oTVL23] a first proyect try to introduce various eye defects into the eye model. It should be emphasized that the project Eyemovie is a computer-manipulated video movie that is the exclusive result of a scientific physical simulation of a 3D human eye model and NOT the result of a computer graphics program. Several models have been designed for ophthalmological refractive studies. In [ATS*13] an optomechanical fluid-filled eye model with dimensions consistent with the human eye was designed and fabricated. This model was compared with the widely used Navarro's model and using ray tracing techniques.

2.2. Depth of Field

Depth of field is critical in the study of eye vision and refractive error. A Ray Tracing based model is presented by Zilong Wang and Shuangjiu Xiao [WX13]. We derive special inspiration from it. Another interesting work is [NKS*13], as it shows real time depth of field simulation using ray tracing. Our model offers a different approach to depth of field simulation. We use the OptiX SDK 7.6 NVIDIA version to compute the scene rendering. An original paper about Optix ray tracin engine is in [PBD*10].

3. Human Eye Model

The visual effect native to the human eye's physiology that makes it differ from the pin hole camera approach is real depth of field

DOI: 10.2312/ceig.20231144

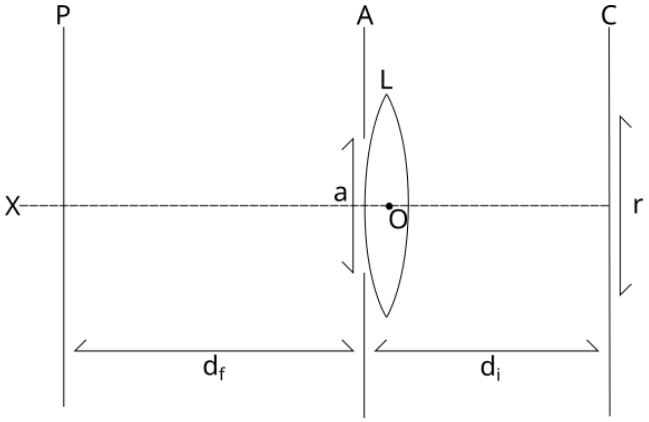

Figure 1: *Schematic view of the proposed model. For visualization purposes L is not included in A plane. As the model describes, L is geometrically included in the A plane.*

simulation. It is the base and most important effect for human vision simulation and for refractive effects to alter it. To be able to render graphics in real time and reduce the amount of calculations involved in the rendering process we have opted for a paraxial approximation in which we only consider a single refractive surface. We are talking about a paraxial reduced eye model. This classification is based on the schematic eye classification model described in [ET18]. A more complex schematic eye approximation would affect performance.

The eye model is based on three parallel planes. P represents the focus plane. It is the area of the field of view which can be seen with the most sharpness. The rest of the field of view volume is distributed around P. A represents the lens plane, the plane where the lens and iris are located. L represents the lens and O the origin of the lens plane and L. a represents the opening of the iris (which is the pupil) in meters. C is the plane where the retina is located. r represents the radius of the retina and is measured in meters. P is d_f meters away from A and A is d_i meters away from C. It is graphically represented in Fig. 1.

The retina is model through a discretization of its space. We determine the retina as a rectangular grid of same size squares projected on plane C's space. We directly map this discretization to the viewport. In accordance, the grid of the retina has the same resolution as the viewport. r ends up as the diagonal of the rectangle that contains the grid of the retina. This can be seen in Figure 2.

The ray tracing process starts by selecting a point on the retina i. A main ray is projected from i to O into object space, where it will find an intersection with the plain P. We call this intersection p. Once we discover this point we distribute the rays' origins among the lens L in accordance to the iris' opening a and we trace the toward p. All generated rays will form a volume. The sections of the volume made from parallel planes to P represent the circle of confusion attributed to the pixel. This way we manage to generate the depth of field effect. This process is graphically represented in Fig. 3.

This process repeats for all pixels according to the discretization

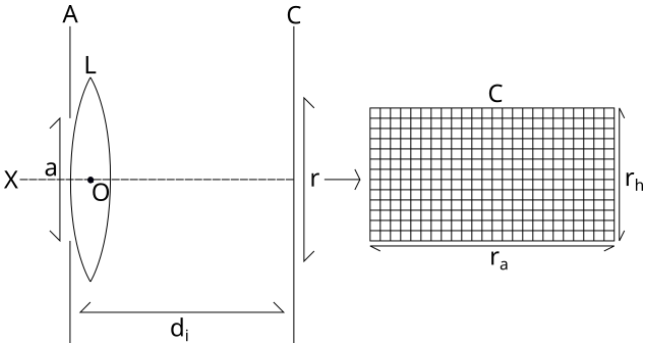

Figure 2: *Discretization of the retina. Notice how r_a and r_h equal to the resolution of the viewport.*

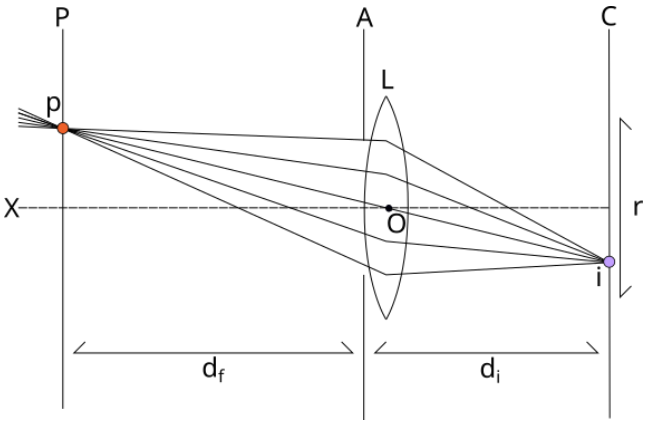

Figure 3: *Graphical representation of the rays traced and intersection point p for a certain pixel i.*

of the retina. Assuming pixel independence each pixel can be calculated by a different parallel process. The final *RGB* value of each pixel will be determined by the average of the values returned by each ray traced. To distribute the rays' origins we have divided the lens radius in n subdivisions and we have also divided it in m diameters separated by a certain phase α (where $\alpha = \frac{PI}{m}$). The number of traced rays are $n_{rays} = n * m + 1$. The interpretation of the distribution is shown in Fig. 4.

Field of view is determined by the values of d_i and r. The greater d_i is, the smaller the field of view. In contrast, the greater r is, the greater the field of view. This effect can be appreciated in Fig. 5.

4. Geometric Defects

To determine all geometric defects, we contrast the physical conditions of the eye under study to an ideal eye. The parameters of the ideal eye are its natural length and the minimum focusable object distance or near point -which increases with age as presbyopia's effect worsens-.

Myopia and hyperopia are easily simulated thanks to the far and near points. These points allow us to simulate the optical capabilities of the eye's accommodation process as the eye has a max-

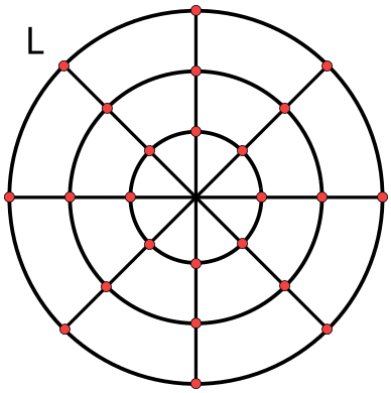

Figure 4: *Distribution of rays' origins across L. Red intersection dots represent these origins. Notice how L's radius is determined by a.*

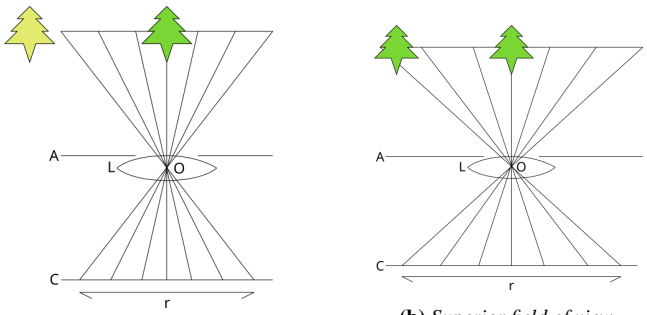

(a) *Inferior field of view.* **(b)** *Superior field of view.*

Figure 5: *Comparative between the field of view depending on the size of r.*

imum and minimum power capabilities. Any object that lies between these two points will be allow the eye to focus it. The focus plane P can only be in the range comprised between of the near and far point, both included. Fig. 6 shows their graphical representation.

Near and far points are calculated usig the formulae:

$$P_{min} = \frac{1}{f_{max}} = \frac{1}{length_{eye}}$$

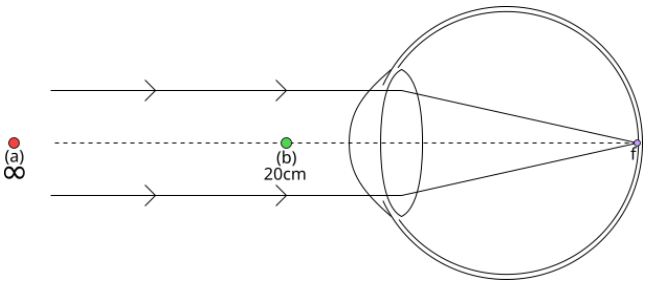

Figure 6: *Graphical representations of far (a) and near (b) points.*

$$P_{max} = \frac{1}{f_{min}} = \frac{1}{length_{eye}} + \frac{1}{NP_{ideal}}$$

$$\Delta P = P_{min} - P'_{min}$$

$$FP = \Delta P^{-1}$$

$$NP = (AA + \Delta P)^{-1}$$

where P_{mim} and P_{max} are the minimum and maximum power of the eye, ΔP is the difference between the minimum power of the ideal eye P'_{min} and the eye under study P'_{min}, FP is the far point and NP is the near point.

Our approach has some limitations. When both the far and near point values are infinite we lack the real effect of the circle of confusion, as we assume that the object we're looking at is always positioned at an infinite distance. This causes the same vision that an unaccommodated eye would have.

We propose a method to model corneal regular astigmatism based on an additional element introduced into the proposed model. It's based on the assumption that the cornea is divided with two axis 90º away from each other. Each axis has its own refractive error. The previous formulae is updated in accordance to:

$$\Delta P = P_{min} - P'_{min} + P_{axis_{min}}$$

$$P_{axis_{real}} = P_{axis_{max}} - P_{axis_{min}}$$

where $P_{axis_{min}}$ is the power of the axis with the lowest refractive error, and $P_{axis_{max}}$ is the power of the axis with the highest refractive error.

A new focus plane P' is used to determine where the rays of the axis with the highest error converge. The ray tracing process starts by selecting a point on the retina i. A main ray is projected from i to O into object space, where it will find an intersection with the plain P'. We call this intersection p'. Once we discover this point we distribute the rays' origins among the lens L in accordance to the pupil opening. For each of these new origins we calculate their projection onto the axis with the highest error in lens space. A ray is traced from this new origin towards p'. A new intersection point with P is obtained. The definitive ray is traced form its previous origin towards the recently obtained p_{ij} intersection point. This process is graphically shown in Fig. 7.

5. Color Defects

To model color defects in a post processing is the fastest option. Otherwise, we should model the chemistry and physics involved in the retina's determining of the light frequency. The clearest way is to apply a function to every screen pixel once we have obtained the render result. This function is defined as a matrix product between a color transformation matrix and the render's result *RGB* expressed as:

$$\begin{pmatrix} R'_{ij} \\ G'_{ij} \\ B'_{ij} \end{pmatrix} = \begin{pmatrix} r_1 & r_2 & r_3 \\ g_1 & g_2 & g_3 \\ b_1 & b_2 & b_3 \end{pmatrix} \begin{pmatrix} R_{ij} \\ G_{ij} \\ B_{ij} \end{pmatrix}$$

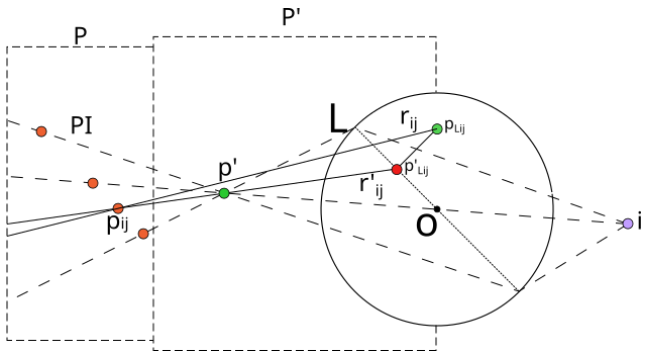

Figure 7: *Graphical representations of the ray tracing process adapted to astigmatism simulation.*

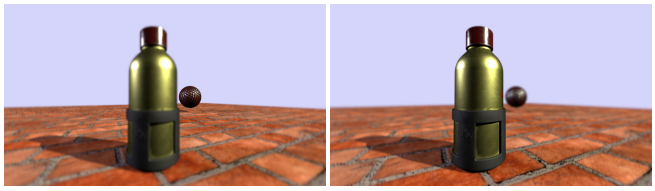

(a) *Focusing far object.* **(b)** *Focusing close object.*

Figure 8: *Depth of field comparison.*

This transformation is applied to each color pixel (right) to determine its new value after color blindness (left). Matrix values may vary for each condition. The simplest and clearest case is the nonexistence of color defects. In this case, the identity matrix is used as the color transformation matrix.

6. Scene Rendering

To render the scene we have used a traditional Ray Tracing approach. How rays travel across the screen and the way they generate new rays to calculate their contribution is as described by Turner Whitted [Whi80]. The main difference is based on how rays originate and which direction they take in accordance to the proposed camera model. The final value of each pixel is the average of all pixels traced as described in previous sections. To speed up scene rendering process heavy parallelization is involved. A GPU core should be dedicated to each ray at generation time for real time rendering. The higher the number of samples, the higher the algorithm's computational cost. Based on our approach, each pixel is independent from each other.

7. Results

A comparison between different results will be shown by changing certain parameters. If no refractive error is specified there is none. How the focus plane and iris radius affects depth of field can be seen in Fig. 8. How *a* affects depth of field in Fig. 9. How field of view changes based on *r* in Fig. 10. Hyperopia in Fig. 11. Myopia in Fig. 12. Astigmatism in Fig. 13. Color blindness cases in Fig. 14.

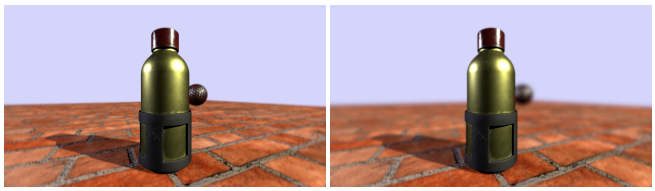

(a) *a = 4mm.* **(b)** *a = 18mm*

Figure 9: *Iris diameter opening a comparison. Notice how depth of field effect intensifies as the iris opens.*

(a) *r = 36mm.* **(b)** *r = 60mm.* **(c)** *r = 100mm.*

Figure 10: *Field of view comparison altering retina diagonal r.*

8. Conclusions & Future Work

We have described a way to simplify and model human eye accommodation process and color defects maintaining a high degree of realism. This approach allows for real time rendering. Future work involves improving on the hyperopia edge case. A change on rays' trajectories according to the eye's global refractive defect would be fitting. Rays would diverge instead of converging at a certain point as no focus plane would be possible to form in the eye's accommodation range. To model color defects more faithfully an improved simulation of the chemical processes involved in retinal color detection would be a realistic approach, but it would suppose a higher computational cost in comparison to traditional post processing methods as described in this paper. From a medical point of view, the results have been evaluated by ophthalmologists with the aim of using them as a reference for the selection of specific refractive lenses, showing patients what image quality they will have after the operation. In a future study it is desired to extend this validation with more users and different visual defects.

References

[ATS*13] ARIANPOUR A., TREMBLAY E. J., STAMENOV I. N., FORD J. E., SCHANZLIN D. J., LO Y.-H.: An optomechanical model eye for ophthalmological refractive studies. *Journal of refractive surgery 29 2* (2013), 126–32. 1

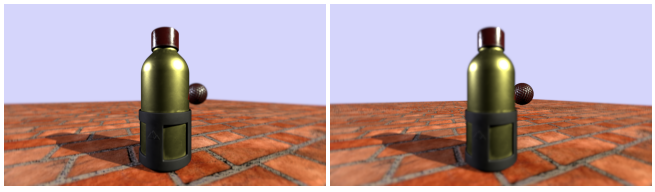

(a) *-2.5D.* **(b)** *-5D.*

Figure 11: *Hyperopia defect comparison. The eye is trying to focus the close object.*

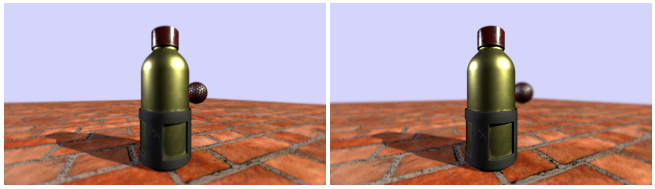

(a) *2.5D.* **(b)** *5D.*

Figure 12: *Myopia defect comparison. The eye is trying to focus the far object.*

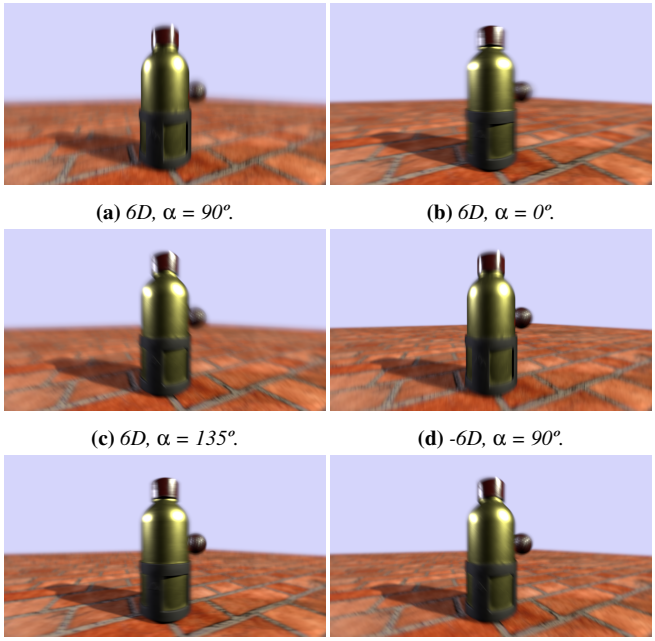

(a) *6D,* $\alpha = 90º$. **(b)** *6D,* $\alpha = 0º$.

(c) *6D,* $\alpha = 135º$. **(d)** *-6D,* $\alpha = 90º$.

(e) *-6D,* $\alpha = 0º$. **(f)** *-6D,* $\alpha = 135º$.

Figure 13: *Astigmatism comparison.*

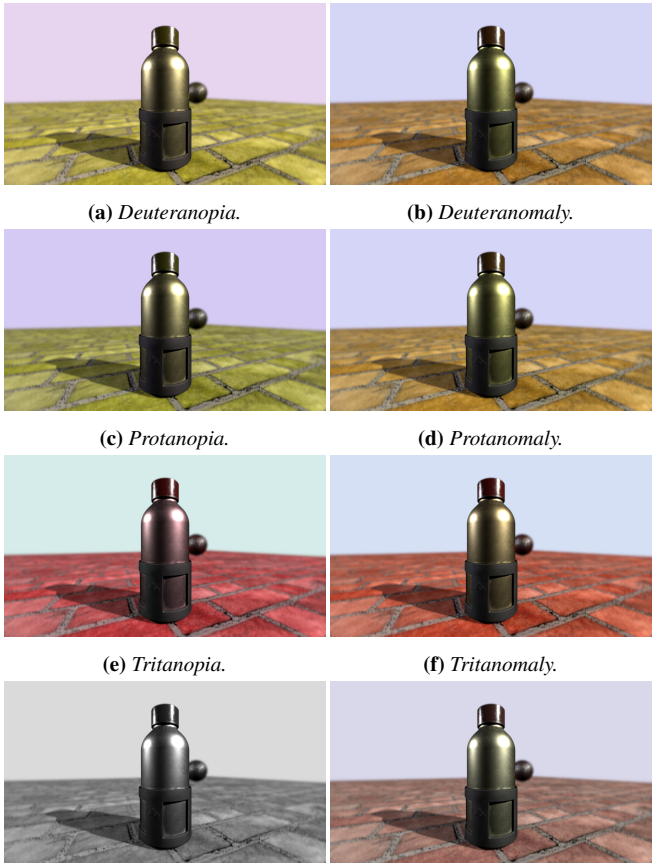

(a) *Deuteranopia.* **(b)** *Deuteranomaly.*

(c) *Protanopia.* **(d)** *Protanomaly.*

(e) *Tritanopia.* **(f)** *Tritanomaly.*

(g) *Achromatopsia.* **(h)** *Achromatomaly.*

Figure 14: *Color blindness effect comparison.*

[ET18] ESTEVE-TABOADA JOSÉ J. M.-M. R. F.-B. T.: Schematic eye models to mimic the behavior of the accommodating human eye. *Journal of Cataract Refractive Surgery 44*, 5 (May 2018), 627–727. doi:10.1016/j.jcrs.2018.02.024. 2

[NKS*13] NIESSNER M., KUHNERT N., SELGRAD K., STAMMINGER M., MICHELSON G.: Real-time simulation of human vision using temporal compositing with cuda on the gpu. In *Proceedings 25th Workshop on Parallel Systems and Algorithms 2013* (2013). 1

[NSB85] NAVARRO R., SANTAMARÍA J., BESCÓS J.: Accommodation-dependent model of the human eye with aspherics. *J. Opt. Soc. Am. A 2*, 8 (Aug 1985), 1273–1280. URL: https://opg.optica.org/josaa/abstract.cfm?URI=josaa-2-8-1273, doi:10.1364/JOSAA.2.001273. 1

[oTVL23] OF TECHNOLOGY VISUAL C. I., LABORATORY A. E. S. R.: Project "eyemovie": Motion visualization of eye defects, 2023. URL: https://www.vaesrl.com/content/project-eyemovie-motion-visualization-eye-defects. 1

[PBD*10] PARKER S. G., BIGLER J., DIETRICH A., FRIEDRICH H., HOBEROCK J., LUEBKE D., MCALLISTER D., MCGUIRE M., MORLEY K., ROBISON A., STICH M.: Optix: A general purpose ray tracing engine. URL: https://doi.org/10.1145/1778765.1778803, doi:10.1145/1778765.1778803. 1

[Whi80] WHITTED T.: An improved illumination model for shaded display. *Commun. ACM 23*, 6 (jun 1980), 343–349. URL: https://doi.org/10.1145/358876.358882, doi:10.1145/358876.358882. 4

[WX13] WANG Z., XIAO S.: Simulation of human eye optical system properties and depth of field variation. *International Journal of Machine Learning and Computing 3* (2013), 413–418. 1

[WZHX11] WU J., ZHENG C., HU X., XU F.: Realistic Simulation of Peripheral Vision Using An Aspherical Eye Model. In *Eurographics 2011 - Short Papers* (2011), Avis N., Lefebvre S., (Eds.), The Eurographics Association. doi:10.2312/EG2011/short/037-040. 1